ISSN 1027-5495. Functional Materials, 32, No.4 (2025), p. 705-714
doi:http://dx.doi.org/10.15407/fm32.04.705

3D printing of a scintillation element for thermal neutron detection based on $ZnS{:}Ag/B_2O_3$

M.L. Sibilyev, A.Yu. Boyarintsev, O.V. Kolesnikov, V.O. Novgorodtsev, T.G. Sibilieva

Institute for Scintillation Materials, State Scientific Institution «Institute for Single Crystals» of National Academy of Sciences of Ukraine, 61072 Kharkiv, Ukraine, Nauky Ave., 60

Received July 29, 2005

A new method of creating a multilayer scintillation element for the registration of thermal neutrons using 3D printing technology on an FDM printer has been developed. The influence of thermophysical parameters of printing materials on the geometric shape and functional properties of the printed product was investigated. Optimal settings of the printing technology were selected. Samples of the scintillation element, which consists of layers of light guides alternating with scintillator layers, have been produced. Polystyrene was used as the light guide. A composite material based on polystyrene with a filler of zinc sulfide powder activated by silver, with the addition of a boron oxide (B_2O_3) neutron converter – $ZnS{:}Ag/B_2O_3$ – was used as a scintillator. The use of 3D printing with two materials in a single technological cycle made it possible to significantly simplify the process of creating a scintillation element compared to traditional technologies. The thermal neutron registration efficiency of the scintillation element sample created using 3D printing technology is 68%, which is comparable to the modern analogs of solid-state detectors created using traditional technology.

Keywords: 3D printing, FDM, ZnS:Ag, boron oxide, neutron converter, scintillation material, scintillation element, efficiency of thermal neutron registration, thermophysical parameters

3Д-друк сцинтиляційного елемента для детектування теплових нейтронів на основі $ZnS{:}Ag/B_2O_3$. *М.Л. Сібілєв, А.Ю. Бояринцев, О.В. Колесніков, В.О. Новгородцев, Т.Г. Сібілєва*

Розроблено новий спосіб створення багатошарового сцинтиляційного елементу для реєстрації теплових нейтронів з використанням технології 3D-ддруку на FDM принтері. Досліджено вплив теплофізичних параметрів матеріалів друку на геометричну форму та функціональні властивості друкованого виробу. Підібрано оптимальні налаштування технології друку. Виготовлено зразки сцинтиляційного елементу, який складається з шарів світловодів, що чергуються з шарами сцинтилятору. В якості світловодів використано полістирол. В якості сцинтилятору використано композитний матеріал на основі полістиролу, з наповнювачем порошку сульфіду цинку, активованого сріблом з додаванням конвертеру нейтронів нейтронів оксиду бору B_2O_3 – $ZnS{:}Ag/B_2O_3$. Використання 3D-друку двома матеріалами в єдиному технологічному циклі дозволило значно спростити процес створення сцинтиляційного елементу порівняно до традиційних технологій. Ефективність реєстрації теплових нейтронів зразку сцинтиляційного елемента, створеного за технологією 3D-друку, становить 68%, що можна порівняти з сучасними аналогами твердотільних детекторів, створених за традиційною технологією.

1. Introduction

Thermal neutron detectors are used in radiation portal monitors [1, 2, 3], nuclear power engineering [4], neutron radiography [5], etc. Due to the combination of high functional and operational characteristics, gas proportional detectors based on ^3He have found wide application and have become the de facto standard in this field. However, over the last ten years, there has been a shortage and rising prices of this isotope. The annual production of ^3He is 10-20 thousand liters, while the demand is 40-70 thousand liters [2]. This necessitates the introduction of alternative thermal neutron detectors, in particular solid-state scintillation detectors. Usually, such detectors contain neutron converters – isotopes capable of efficient absorption of neutrons with subsequent emission of alpha particles, which, in turn, interact with the scintillator (for example, ZnS:Ag). Despite the fact that such detectors have been known for more than half a century [6], the development of such detectors is currently still relevant. They are considered as one of the promising technologies for replacing ^3He detectors [2, 7]. The most common neutron converters are the isotopes ^6Li and ^{10}B, [3, 7]. Scintillation detectors based on ZnS:Ag with such converters demonstrate technical characteristics comparable to ^3He gas discharge detectors [8-10].

Although ^{10}B is inferior to ^6Li in reaction energy (4.78 MeV versus 2.73 and 2.05 MeV for ^{10}B), it has the following advantages: a larger neutron capture cross section (3837 barn versus 942 barn for 6Li); a higher content of the ^{10}B isotope in natural boron (about 20% compared to 7.5% of ^6Li in natural lithium), which makes it possible to use natural boron for the manufacture of detectors without strict efficiency requirements; a larger number of non-hygroscopic and chemically stable compounds, which determines the manufacturability of scintillation elements.

Since it is currently impossible to obtain bulk crystals of ZnS:Ag, the scintillation material is made in the form of composites and mixtures, which are small granules of ZnS:Ag in a polymer matrix. Obviously, such mixtures have a large extinction coefficient, so they are practically opaque. The traditional way to overcome this drawback is to use designs in which the scintillation signal is transmitted to the photodetector through a non-scintillating fiber. In practice, this principle is implemented in the following designs: detectors in the form of non-scintillating fibers with a scintillation coating [7], ring detectors [11] and more common multilayer detectors in which scintillation layers alternate with optical fiber layers. Depending on the application conditions, detectors with different numbers of scintillator and fiber layers are manufactured [8, 12, 13].

Geometric parameters of scintillation elements are determined by their specific purpose and operating conditions. In the first approximation, it is possible to formulate the following general principles regarding the interrelationship of geometric and functional parameters. Reducing the thickness of the scintillation layer makes it possible to reduce the sensitivity to gamma radiation. Increasing the number of scintillation layers allows for higher neutron detection efficiency. Reducing the thickness of the optical fiber allows for more compact scintillation elements. For example, a scintillation element for thermal neutron detection [12] has 3 layers of light-guiding material with a thickness of 3 mm and 4 scintillation layers with a thickness of 0.2 mm. And the scintillation element for recording thermal neutrons [8] has 4 layers of light- guiding material with a thickness of 3 mm and 5 scintillation layers with a thickness of 0.2 mm.

The idea of manufacturing scintillation detectors using 3D printing methods is relatively new, but has already proven its capabilities in scintillation materials science [14-17]. At the same time, 3D printing methods provide new opportunities for automating production, obtaining products of stable quality and accuracy by eliminating the “human factor”, the relative ease of obtaining geometrically complex prototypes and detectors consisting of several materials, etc. [14, 16, 18].

One of the most common additive manufacturing technologies, Fused Deposition Modelling (FDM), is based on the layer-by-layer deposition of molten material onto a work platform. A thread of low-melting material (filament) is fed into a heated extruder, melted and extruded onto the platform. The extruder moves along a given trajectory, creating a part of a given shape. FDM technology allows creating both monolithic and composite scintillation detectors [14, 17]. This work continues this direction and is devoted to the study of the possibilities of creating scintillation elements from two different (both in terms of thermophysical and functional properties) materials in a single technological cycle.

In contrast to the fabrication of structural parts, when manufacturing optically transparent scintillation elements, it is necessary to select printing parameters that exclude the formation of cavities [19, 20]. The formation of cavities depends on the bonding conditions of adjacent layers, which are determined by the rheological characteristics of the molten filament, the temperature of the extruder and printer table, the thickness of the applied layers, etc. [19-23].

The purpose of the work is to develop a new method of creating a multilayer scintillation element for the registration of thermal neutrons using FDM technology; for this, the following stages must be implemented: 1) develop a suitable compatible pair of materials (composite polymer material based on ZnS:Ag/^{10}B and light-guiding material) in the form of a filament, taking into account the specifics and limitations of FDM technology; 2) investigate the influence of printing parameters on the bonding conditions of polymer layers and on the geometric and functional parameters of the resulting scintillation elements; 3) create a research prototype of a neutron detector using the FDM 3D printing method.

2. Experimental

The technological sequence of obtaining the detector includes the following stages: obtaining scintillation granules ZnS:Ag by the method of solid-phase synthesis; coating the granules with converter material; obtaining scintillation and transparent filament; printing the scintillation element on an FDM printer.

Often, boron oxide (B_2O_3) is used as a converter [5, 6]. This is justified, since the natural content of the isotope ^{10}B in it is 6.3%. This content of the isotope ^{10}B allows the use of boron oxide without additional enrichment.

2.1 Preparation of scintillation material ZnS:Ag *with converter*

The solid-phase synthesis of the ZnS:Ag scintillator is carried out in a sealed crucible, into which carefully dried initial components (ZnS, AgCl, NaCl and S powders) are loaded [24]. The synthesis is carried out in vacuum with a gradual increase in temperature to 820°C. Removal of auxiliary substances (NaCl) and unreacted components is carried out by successive washing with a solution of sodium thiosulfate ($Na_2S_2O_3$) and distilled water. After washing and drying, approximately round ZnS:Ag granules with a characteristic size of 10-20 μm are obtained.

The next step is to create a ZnS:Ag/B_2O_3 scintillation material by coating ZnS:Ag granules with a converter film (B_2O_3) according to [25]. The production of the scintillation composition includes the use of ready-made phosphor ZnS(Ag) and boric acid (H_3BO_3) in a ratio of 2:1 and subsequent sintering of the resulting mixture, crushing and separation into fractions. A layer of boric acid from its heated saturated aqueous solution is deposited on the phosphor grains. The resulting product is separated from the cooled solution and, after drying, sintered at a temperature of 430-470°C. Fractions with particle sizes of up to 50 microns are used, which is acceptable for creating a composite for 3D printing by the FDM method.

2.2 Obtaining filaments for 3D printing

Experience shows that when creating scintillation elements made of two different materials using FDM technology, it is advisable to use polymer matrices with similar thermophysical characteristics. In this work, we use polystyrene (PS) without luminescent additives as a composite matrix for the scintillation filament and for the filament for printing the light guide. PS meets all the necessary requirements: it is transparent in the region of the ZnS:Ag luminescence spectrum (420 nm) and has acceptable values of printing and glass transition temperatures. It was also experimentally established that during the manufacture of composite filaments, different plastics have different degrees of mixing with powders of solid fillers. Thus, polystyrene showed significantly better miscibility (for example, compared to polycarbonate or PMMA). This ensures homogeneity of the mixture with ZnS:Ag granules. For the manufacture of the filament, crushed PS obtained by the method of cast polymerization from the monomer was used.

Filaments with a diameter of 1.75 ± 0.05 mm were produced using a laboratory extruder Noztek Pro HT at a temperature of 200-235°C. Polystyrene granules were used for the production of the light guide filament. A composite material from a mixture of ZnS:Ag granules coated with a layer of B_2O_3, polystyrene granules, and a plasticizer was used to manufacture the scintillation filament [14].

2.3 3D printing

Printing a prototype of a neutron-sensitive detector element involves the sequential creation of a structure consisting of layers of two types: a scintillator and a light guide. The printing format is the formation of layers in one technological process using two different materials. SolidWorks 3D CAD software was used to develop the product model. To divide the developed model into layers for 3D printing, the CreateWare slicer program was used.

The final structure of the scintillation element is similar to the previously developed analogue [12] and is a rectangular parallelepiped with dimensions: length = 40 mm, width = 25 mm, height = 10 mm. The number of scintillator layers is 6 layers, the light guide layer is 5 layers.

For 3D printing, a CREATBOT F430 3D printer with two extrusion heads was used. The printing layer, the temperature of the extrusion and the desktop, the printing speed and other parameters are set depending on the purpose of the experiment and are the subjects of this research. The first layer, 0.2 mm high, was printed with scintillation filament based on polystyrene with the addition of $ZnS:Ag/B_2O_3$. After that, the next layer, 1.7 mm high, is printed with a light-conducting filament made of pure polystyrene. Then, similar iterations were repeated 5 times and the last layer was printed with a scintillation filament.

The manufactured multilayer structure is grinded on all ends. One end (smaller side) is polished to optical transparency. The resulting scintillation element blank is covered on five sides with two layers of 200-µm-thick reflective polytetrafluoroethylene film; the sixth side (polished smaller side) remains free (Fig. 1).

2.4 Modeling heat transfer during printing

Since direct measurements of temperature distribution when printing detectors with thin monolayers present certain technical difficulties, the dynamics of heat exchange processes will be estimated from the data of the mathematical model.

Let'S formulate a model for printing a multilayer sample made of two materials (material A and material B). Let'S introduce the following terms: the material applied in one pass of the 3D printer extruder will be called a monolayer; several monolayers of the same material will be called a layer.

Multilayer detector consists of N_A layers of material *A*, which in turn consists of n_A monolayers, and $N_B = N_A - 1$ layers of material *B*, which in turn consists of $n_{\square}$ monolayers. Each new monolayer is applied to the previous monolayer with a time interval $\tau = const$. The thickness of the monolayers for both materials is $h_m = const$. The temperature of the new monolayer at the time of application at $t = n\tau$ regardless of the material $\mathrm{T} = T_0 = const$.

The boundary condition on the lower surface of the sample at *z=0*

$$T(z=0,t) = T_{base} \tag{1}$$

where T_{base} is the temperature of the 3D printer base (Table).

The boundary condition on the upper surface of the sample *z=Z(t)* corresponds to the cooling of the printed sample due to convection and radiation heat exchange

$$-\lambda_i \frac{\partial T}{\partial z}\Big|_{z=Z(t)} = H_{eff}\left(T\left(Z(t),t\right) - T_{amb}\right) \tag{2}$$

$$Z(t) = mh_m \text{ for } m\tau \le t < (m+1)\tau \tag{3}$$

where, λ is the thermal conductivity coefficient; T_{amb} is the temperature in the 3D printer chamber; H_{eff} is the effective heat transfer coefficient at the upper boundary of the detector being printed; m is the ordinal number of the monolayer; τ is the time interval between applying monolayers; *Z(t)* is the height of the detector being printed at any moment of time *t*.

Between the individual monolayers there is an ideal thermal contact, which fulfills the conditions of continuity of temperature and heat flow

$$T_i\left(z_i(t)^-, t\right) = T_{i+1}\left(z_i(t)^{+,} t\right) \tag{4}$$

$$\lambda_i \frac{\partial T}{\partial z}\Big|_{z_i^-} = \lambda_{i+1} \frac{\partial T}{\partial z}\Big|_{z_i^+} \tag{5}$$

Using the simplification associated with the absence of heat transfer through the side surfaces of the printed sample, we will write down the one-dimensional equation of heat conduction for a multilayer sample

$$\frac{\partial T}{\partial t} = a_i \frac{\partial^2 T}{\partial z^2} \tag{6}$$

$$a_i = \frac{\lambda_i}{c_i \rho_i} \tag{7}$$

$$i = \begin{cases} A, m \in [1, n1] \cup [n2, n3] \cup [n4, n5] \cup [n6, n7] \cup [n8, n9] \cup [n10, n11] \\ B, m \in [n1, n2] \cup [n3, n4] \cup [n5, n6] \cup [n7, n8] \cup [n9, n10] \end{cases} \tag{8}$$

Table 1 Thermophysical parameters of materials

Name	Parameter	Unit of measurement	ZnS:Ag	scintillation filament (i=A)	light guide filament of PS (i=B)
thermal conductivity coefficient	λ	W m^{-1} K^{-1}	27 [30]	3.9	0.13 [31]
density	ρ	kg m^{-3}	4090 [32]	1519	1100 [31]
heat capacity	c	J kg^{-1} K^{-1}	480 [33]	991	1300 [31]
thermal diffusivity	a	m^2 S^{-1}	1.4 10^{-5}	2.6 10^{-6}	9.1 10^{-8}

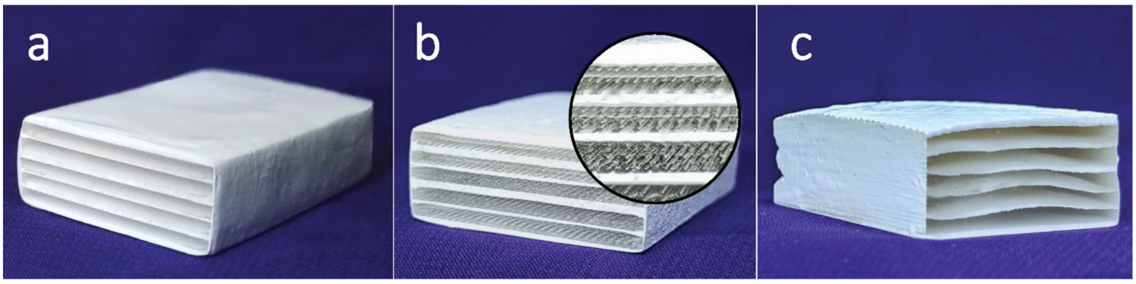

Fig. 1. Variants of neutron-sensitive scintillation elements manufactured using FDM technology

where, $n1, n2 \dots n11$ are the numbers of monolayers of material A (total of 6 scintillation layers) and material B (total of 5 light-guiding layers) in 11 separate layers of the detector with a total size of $n11$ monolayers; a is the thermal conductivity, which is given by a piecewise-continuous function.

Thermophysical parameters of the materials are given in Table 1. These are: λ_i,ρ_i, c_i, a_i where i means the material type of a separate monolayer $i \in \{A,B\}$. All of them are constant and do not depend on temperature.

The glass transition temperature of polystyrene can take different values depending on the method and conditions of polymerization, starting materials, etc. Therefore, in this work, the glass transition temperature of polystyrene used was determined by the method [26, 27]. It consists in measuring the electrical capacitance of samples measuring 40 x 40 x 0.2 mm, placed between polished aluminum plates. The sample is placed in the furnace with a rate of temperature change of 1 K min^{-1}. The glass transition temperature is determined by the position of the breaking point on the graph of capacity versus temperature. The obtained value T_g = 102°C corresponds to the literature data [28, 29]. The electrical capacitance was measured using an immittance meter E7-13.

The density, heat capacity, and coefficient of thermal conductivity of the composite scintillation material are calculated using formulas

$$\rho_{comp} = \rho_{ZnS} p_{ZnS} + \rho_{PS} p_{PS} \tag{9}$$

$$A_{comp} = \frac{\rho_{ZnS} p_{ZnS} A_{ZnS} + \rho_{PS} p_{PS} A_{PS}}{\rho_{comp}} \tag{10}$$

$$\lambda_{comp} = \lambda_{ZnS} p_{ZnS} + \lambda_{PS} p_{PS} \tag{11}$$

where, $\rho_{comp}, \rho_{ZnS}, \rho_{PS}$ are the densities of the composite material, zinc sulfide, and polystyrene, respectively; $A_{comp}, A_{ZnS}, A_{PS}$ are the the heat capacities of the composite material, zinc sulfide, and polystyrene, respectively; $\lambda_{comp}, \lambda_{ZnS}, \lambda_{PS}$ are the coefficients of thermal conductivity of the composite material, zinc sulfide, and polystyrene, respectively; p_{ZnS}, p_{PS} are the mass fractions of zinc sulfide and polystyrene, respectively.

3. Results and discussion

The appearance of the scintillation elements produced according to different technological parameters of printing is shown in Fig. 1. Fig. 1b shows an element with defects typical for FDM printing – cavities (bubbles) in the volume of the light-conducting layers. There are several reasons for the occurrence of this defect: the round shape of the extruder nozzle, the relatively high viscosity of polymer melts, the difficulty of creating thermal conditions for binding adjacent filament threads, the insufficient volume of the material, etc. [19, 20]. Possible methods for eliminating these reasons include increasing the temperature of the extruder and printer table, reducing the thickness of monolayers, increasing the extrusion multiplier, etc. In this case, it is possible to significantly reduce the porosity of the printed parts, but at the

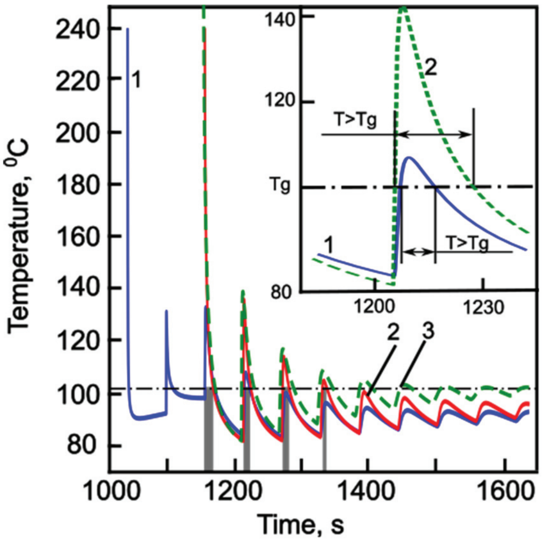

Fig. 2. Modeling of temperature distribution during printing. The effect of changing the temperature of the extruder (T_0) and the surface of the printing bed (T_{base}).

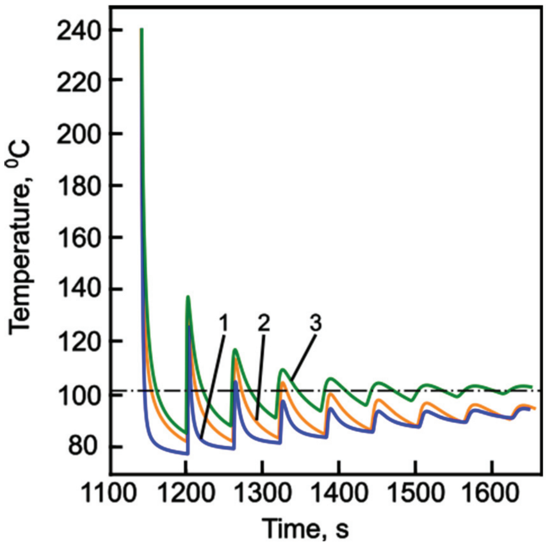

Fig. 3. Modeling of temperature distribution during printing. Effect of changing the heat transfer coefficient (H_{eff})

same time its geometry deteriorates (Fig. 1c). That is, the practical task was to find such a set of technological printing parameters that minimize the number of pores while preserving the geometry of the scintillation element (Fig. 1a).

A series of experiments were conducted on printing detectors with varying the following parameters: heat transfer coefficient H_{eff}, monolayer thickness h_m, table temperature T_{base}, extruder temperature T_0, extrusion multiplier "*Flow*" (percentage of plastic flow intensity through the extruder relative to factory settings). The quality of the manufactured printed detectors was assessed by the following parameters: plane parallelism of scintillation layers; deviation of the external shape of the detector from the specified one; presence of inclusions in the light guide layer. The influence of the above parameters on the temperature distribution was determined from the analysis of the simulation results.

To simplify the quantitative assessment of the relationship between printing modes, it is proposed to introduce a single measurement parameter. Its essence will be the time during which the temperature of the printed layer exceeds the glass transition temperature of polystyrene. First, this parameter is naturally associated with print modes. Second, it determines the conditions for bonding monolayers and the formation of bridges between rows of plastic mass [20]. This affects the optical characteristics of the light-guiding layer. Thirdly, it determines the volume of the already printed layer, which is subjected to deformations due to the movement of the extruder and the pressure of new portions of the molten material. This determines the degree of deviation of the geometric dimensions from the specified ones.

A fragment of the calculation of temperature changes during printing is shown in Fig. 2. Curve 1 (blue) in Fig. 2 corresponds to the printing of a scintillation layer consisting of two monolayers. Curve 2 (red) in Fig. 2 corresponds to the printing of a light guide layer with the optimal set of parameters (Fig. 1a): extruder temperature T_0 = 240 °C, table temperature T_{base} = 100 °C. The dash-dotted line indicates the glass transition temperature. The glass transition "temperature overshoot time" parameter is equal to the sum of the gray rectangles. Curve 3 in Fig. 2 corresponds to the printing mode T_0 = 250 °C, T_{base} = 110 °C. Increasing the extruder temperature by 10 °C to T_0 = 250 °C causes a slight increase in temperature in the first 100 - 150 seconds (nearest 2 - 3 layers) after application. This is due to the fact that the main heat flow is directed upwards (heat transfer to the 3D printer chamber). When the table temperature is increased by 10 °C to T_{base} = 110 °C, a constant increase in temperature is observed approximately 200 seconds after application (there are already 5-6 layers to the sample surface). The time of exceeding the glass transition temperature is significantly increased. The light guide layer of the printed element will be almost free of cavities, but the plane parallelism of the scintillation layers is lost, and the external dimensions

Table 2. Calculated and measured parameters of scintillation elements

Parameter	Unit	Value	Time $T>T_g$, sec	Layer geometry deviation, mm	Product geometry deviation, mm	Presence of cavities in the volume	Product example
H_{eff}	$W\ m^{-2}\ K^{-1}$	10	76	1.5-2	3-4	insignificant	
H_{eff}	$W\ m^{-2}\ K^{-1}$	50	21	up to 0.5	up to 1.5	multiple	Fig. 2b
h_m	mm	0.05	13	up to 0.5	up to 1.5	multiple	
h_m	mm	0.2	48	up to 1	1-2	little	
T_0	°C	230	27	up to 0.3	up to 1.0	multiple	
T_0	°C	250	42	1-2	4-5	missing	Fig. 2c
T_{base}	°C	90	25	up to 0.5	up to 1.5	medium	
T_{base}	°C	110	89	up to 1	2-3	insignificant	
Flow	%	100	38	up to 0.3	up to 1.0	much a lot	
Flow	%	120	38	1.5-2	3-4	missing	

deviate from the specified ones by more than 4-5 mm (Fig. 1c).

The effect of changing the heat transfer coefficient on the time of exceeding the glass transition temperature is shown in Fig. 3. An increase in the heat transfer coefficient (curve 1, Fig. 3) above the optimal mode (curve 2, Fig. 3) leads to a significant decrease in the time it takes to exceed the glass transition temperature. This printing mode corresponds to the element shown in Fig. 1b. Decreasing in the heat transfer coefficient (curve 3 Fig. 3) significantly increases the time of exceeding the glass transition temperature, which leads to a result similar to that described in the previous paragraph.

To determine the effect of thermal destruction of polystyrene and its oxidation by oxygen in the air during the manufacture of the filament and during printing, samples measuring 25 mm x 40 mm x 1.7 mm were made from polystyrene by cast polymerization method and obtained by 3D printing. The absorption spectrum was measured on a spectrophotometer Shimadzu UV-2450. It was found that the absorption spectrum in the ultraviolet region shifts by approximately 40 nm. At the same time, in the region of 420 nm, corresponding to the luminescence of ZnS:Ag, the absorption coefficient remains practically unchanged. The results are given in Fig. 4. Similar results were obtained in [34, 35]. Thus, it was established that the thermal effects associated with filament production and 3D printing do not prevent the use of polystyrene with scintillation materials based on ZnS:Ag.

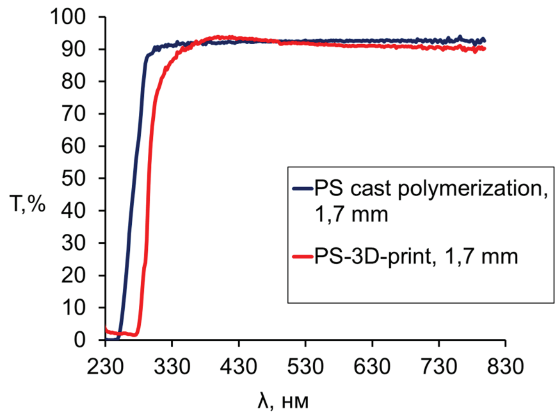

Fig. 4. Comparison of light absorption spectra of polystyrene produced by cast polymerization with polystyrene samples printed on an FDM 3D printer.

The results of experiments and calculations are summarized in Table 2.

The best obtained scintillation element (Fig. 2a), manufactured with the following set of printing parameters, was chosen as a reference sample: H_{eff} =30 $W\ m^{-2}\ K^{-1}$, h_m = 0.1 mm, T_0 = 240 °C, T_{base} = 100 °C time. The calculated parameter (time of exceeding the glass transition temperature) $T> T_g$ = 38 S. *Flow* = 110%. The quality indicators for it: deviation from the specified layer geometry is less than 0.3 mm; deviation from the specified product geometry is less than 1.0 mm; the presence of cavities in the volume of the light-guiding layers is insignificant.

Measurement of thermal neutron detection efficiency of a printed scintillation element based on $ZnS:Ag/B_2O_3$

To measure the neutron registration efficiency (η_n), a printed scintillation layer made of a composite material based on $ZnS:Ag/B_2O_3$ and a scintillation element made of 6 such layers were installed directly on the entrance window of the photomultiplier (PMP) on the side free of the reflective coating. The neutron registration efficiency (η_n) was measured on a device with a CAEN 5770 multichannel analyzer, a Hamamatsu R1307 photomultiplier (PMP) and a certified 239Pu-Be fast neutron source with a flux of $1 \cdot 10^5$ n/S ±10% according to the passport. To obtain thermal neutrons, the 239Pu-Be source was placed in the center of a spherical polyethylene neutron moderator with a diameter of 150 mm and a certified conversion factor of fast neutrons to thermal neutrons (8% with an error of ± 5%). Thermal neutrons are absorbed by a screen (1 mm thick) made of metallic cadmium with a natural isotopic composition. The neutron counting rate is measured with and without cadmium. The difference in the resulting counting rates ("cadmium difference") is the thermal neutron counting rate. The ratio of this value to the calculated value of the thermal neutron flux through a layer of scintillation material is the thermal neutron detection efficiency (η_n). Fig. 5 shows the amplitude spectrum obtained by irradiating a scintillation element manufactured by 3D printing using FDM technology. As a result, the area under the difference spectrum reflects the number of thermal neutrons that passed through the entrance window of the detector.

The choice of the distance between the neutron source and the detector is a matter of compromise. The magnitude of the non-uniformity of the neutron flux over the detector area, the proportion of neutrons reflected from the walls of the room, the scattering of neutrons in the air, etc. depend on this distance [36]. Based on considerations of minimizing measurement errors, we chose a distance of 0.3 m. Parameters of the experiment for measuring the thermal neutron detection efficiency: exposure is 1000 S; solid angle of incidence is π/283. Area in the "cadmium difference" spectrum is 4790 counts. Estimated total error of the experiment is about ±16%.

The results of the measurements showed that the printed scintillation layer made of a composite material based on $ZnS{:}Ag/B_2O_3$ with dimensions of 40x25x0.2 mm has a thermal neutron detection efficiency of 17%. The printed detector has a thermal neutron detection efficiency of 68%, which is 91% of the efficiency compared to the analog created by traditional methods based on the scintillation material $^6LiF/ZnS(Ag)$ [8].

Further development of technology for manufacturing layered neutron-sensitive scintillation elements by additive methods (3D printing) has a promising continuation with the use of more efficient materials (for example, composites based on ZnS:Ag/carborane according to [12]). These directions could form the basis for new research into the use of 3D printing to create detectors.

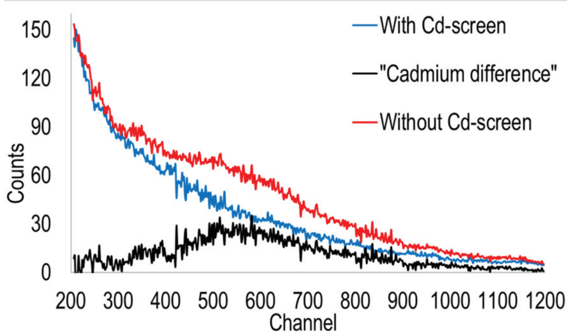

Fig. 5. Pulse height spectra of a detector with 6 layers of $ZnS(Ag)/B_2O_3$, subjected to neutron irradiation from a 239Pu-Be source: red curve – without a Cd screen, blue curve – with a Cd screen, black curve – "Cd difference".

4. Conclusions

A new method for creating a multilayer scintillation element for detecting thermal neutrons using 3D printing technology on an FDM printer has been developed. Filaments of a pair of materials with coordinated thermal properties for 3D printing were manufactured: scintillating composite based on scintillating material $ZnS{:}Ag/B_2O_3$ dispersed in a polystyrene matrix and non-scintillating light-guiding (polystyrene). The influence of thermophysical properties of the materials and technological parameters on the geometric and functional characteristics of the manufactured scintillating elements was investigated. A single measurement parameter has been established: the time during which the temperature of the printed layer exceeds the glass transition temperature of polystyrene. For an optimal balance between optical transparency and geometric accuracy, this value should be within 35-45 S. According to the developed method, a scintillation element consisting of five layers of light-guiding material alternating with six layers of scintillation material was produced. The efficiency of thermal neutron detection of the developed scintillating element is at the level of 68%.

The printed scintillation element based on the $ZnS{:}Ag/B_2O_3$ material can be used to create efficient thermal neutron detectors for high-energy physics, nuclear energy, environmental monitoring, and other fields of science and technology.

References

1. M.G. Paff, S.D. Clarke, R.T. Kouzes, и S.A. Pozzi, «Fast and thermal neutron detectors for radiation portal monitors», IEEE Nuclear Science Symposium and Medical Imaging Conference (NSS/MIC), 2017. doi: 10.1109/NSSMIC.2017.8532639.
2. Kouzes, Richard T. "The 3He Supply Problem." (PNNL-18388), Pacific Northwest National Lab., Richland, WA (United States), May 2009. https://doi.org/10.2172/956899
3. K.A. Guzman-Garcia, H.R. Vega-Carrillo, E. Gallego, J.A. Gonzalez-Gonzalez, A. Lorente, S. Ibañez-Fernandez, «^{10}B+ZnS(Ag) as an alternative to ^{3} He-based detectors for Radiation Portal Monitors», *EPJ Web Conf.*, т. 153, с. 07008, 2017, doi: 10.1051/epjconf/201715307008.
4. B.M. van der Ende, L.Li, D.Godin, B.Sur, «Standoff nuclear reactor monitoring with neutron detectors for safeguards and non-proliferation applications», *Nat. Commun.*, vol. 10, Article number: 1959 (2019), doi: 10.1038/s41467-019-09967-4.
5. T. Kojima, M. Katagiri, N. Tsutsui, K. Imai, M. Matsubayashi, и K. Sakasai, «Neutron scintillators with high detection efficiency», *Nucl. Instrum. Methods Phys. Res. Sect. Accel. Spectrometers Detect. Assoc. Equip.*, vol. 529, is. 1–3, 21 August 2004, p. 325-328, doi: 10.1016/j.nima.2004.05.005.
6. T. Tojo, T. Nakajima, «Preparation of thermal neutron scintillators based on a mixture of ZnS(Ag), 6LiF and polyethylene», *Nucl. Instrum. Methods*, vol. 53, p. 163–166, 1967, doi: 10.1016/0029-554X(67)91347-X.
7. R.T. Kouzes, J.H. Ely, L.E. Erikson, W.J. Kernan, D.C. Stromswold, M.L. Woodring, «Full Scale Coated Fiber Neutron Detector Measurements», PNNL-19264, 976988, 2010. doi: 10.2172/976988.
8. V. Tarasov, O. Zelenskaya, O. Shpilinskaja, L. Trefilova, L. Andruschenko, L. Borysova, Yu. Hapon., «Preparation and characterization of 6LiF/ZnS(Ag) scintillator with varying granulometry», *Funct. Mater.*, vol. 31, p. 153–162, 2024, doi: 10.15407/fm31.02.153.
9. J. Siebach, « Characterization of He-3 Detectors Typically Used in International Safeguards Monitoring», Department of Physics and Astronomy Brigham Young University, Bachelor'S thesis, August 2010.
10. Richard T. Kouzes, James H. Ely, Luke E. Erikson, Warnick J. Kernan, Azaree T. Lintereur, Edward R. Siciliano, Daniel L. Stephens, David C. Stromswold, Renee M. Van Ginhoven, Mitchell L. Woodring, «Neutron detection alternatives to 3He for national security applications», *Nucl. Instrum. Methods Phys. Res. Sect. Accel. Spectrometers Detect. Assoc. Equip.*, vol.. 623, is. 3, p. 1035–1045, 2010, doi: 10.1016/j.nima.2010.08.021.
11. T. Gürdal, H. Yücel, «Design and Development of a Portable Neutron Detection System Based on a 6Li-Doped ZnS(Ag) Scintillator», *Nucl. Technol.*, vol. 211, is. 5, p. 1056–1065, 2025, doi: 10.1080/00295450.2024.2370701.
12. P.M. Zhmurin, V.L. Cherginets, V.O. Tarasov, A.Yu. Boyarintsev, T.G. Sibilieva, M.L. Sibiliev, D.A. Yelisieiev, O.V. Yelisieieva, V.D. Alekseev, Yu.O. Hurkalenko, «Scintillation element for thermal neutron registration», *Funct. Mater.*, 2025; 32 (2): 272-276, doi:https://doi.org/10.15407/fm32.02.272
13. Sean Stave, Mary Bliss, Richard Kouzes, Azaree Lintereur, Sean Robinson, Edward Siciliano, Lynn Wood, «LiF/ZnS neutron multiplicity counter», *Nucl. Instrum. Methods Phys. Res. Sect. Accel. Spectrometers Detect. Assoc. Equip.*, vol. 784, p. 208–212, 2015, doi: 10.1016/j.nima.2015.01.039.
14. T. Sibilieva, V. Alekseev, S. Barsuk, S. Berns, E. Boillat, I. Boiaryntseva, A. Boyarintsev, A. Carbone, A. De Roeck, S. Dolan, T. Driuk, A. Gendotti, I. Gerasymov, B. Grynyov, S. Hugon, U. Kose, O. Opolonin, A. Rubbia, D. Sgalaberna, M. Sibilyev, S. Tretyak, T. Weber, J. Wuthrich, X. Zhao, «3D printing of inorganic scintillator-based particle detectors», 2023, JINST 18, P03007. https://doi.org/10.1088/1748-0221/18/03/P03007
15. S. Berns, A. Boyarintsev, S. Hugon, U. Kose, D. Sgalaberna, A. De Roeck, A. Lebedynskiy, T. Sibilieva, P. Zhmurin, «A novel polystyrene-based scintillator production process involving additive manufacturing», *J. Instrum.*, vol. 15, is. 10, 2020, doi: 10.1088/1748-0221/15/10/P10019.
16. Ł. Kapłon a b c, D. Kulig a, S. Beddar d, T. Fiutowski f, W. Górska a f, J. Hajduga and others, «Investigation of the light output of 3D-printed plastic scintillators for dosimetry applications», *Radiat. Meas.*, vol. 158, p. 106864, 2022, doi: 10.1016/j.radmeas.2022.106864.
17. T. Weber, A. Boyarintsev, U. Kose, B. Li, D. Sgalaberna, T. Sibilieva and others, «Additive manufacturing of a 3D-segmented plastic scintillator detector for tracking and calorimetry of elementary particles», *Commun. Eng.*, vol. 4, is. 1, p.1–11, 2025, doi: 10.1038/s44172-025-00371-z.
18. N. Lynch, T. Monajemi, J. L. Robar, «Characterization of novel 3D printed plastic scintillation dosimeters», *Biomed. Phys. Eng. Express*, vol. 6, is. 5, p. 055014, 2020, doi: 10.1088/2057-1976/aba880.
19. L. Tumarchenko и Y. Vyshnepolskyi, «Evaluation of Fused Deposition Modelling process parameters influence on the porosity of printed parts», *Mech. Adv. Technol.*, vol. 8, is. 3(102),

2024, doi: 10.20535/2521-1943.2024.8.3(102).31 1016.

20. T.D. Ngo, A. Kashani, G. Imbalzano, K.T.Q. Nguyen, D. Hui, «Additive manufacturing (3D printing): A review of materials, methods, applications and challenges», *Compos. Part B Eng.*, vol. 143, p. 172–196, 2018, doi: 10.1016/j.compositesb.2018.02.012.
21. Q. Sun, G.M. Rizvi, C.T. Bellehumeur, P. Gu, «Effect of processing conditions on the bonding quality of FDM polymer filaments», *Rapid Prototyp. J.*, vol. 14, is. 2, p. 72–80, 2008, doi: 10.1108/13552540810862028.
22. C. Bellehumeur, L. Li, Q. Sun, P. Gu, «Modeling of Bond Formation Between Polymer Filaments in the Fused Deposition Modeling Process», *J. Manuf. Process.*, vol. 6, is. 2, p. 170–178, 2004, doi: 10.1016/S1526-6125(04)70071-7.
23. A. Kallel, I. Koutiri, E. Babaeitorkamani, A. Khavandi, M. Tamizifar, M. Shirinbayan, A. Tcharkhtchi, «Study of Bonding Formation between the Filaments of PLA in FFF Process», *Int. Polym. Process.*, vol. 34, is. 4, p. 434–444, 2019, doi: 10.3139/217.3718.
24. Mehdi Sohrabi, Fereshteh Saheli, Kheirollah Mohammadi, «Synthesis of Silver-Activated Zinc Sulfide (ZnS:Ag) Powder by Thermal Diffusion Method for Production of Thin Film Alpha Scintillators», Journal of Nuclear Energy Science & Power Generation Technology, 2018, 7:2, doi: 10.4172/2325-9809.1000182
25. K. Fukao и Y. Miyamoto, «Glass transitions and dynamics in thin polymer films: Dielectric relaxation of thin films of polystyrene», *Phys. Rev. E*, т. 61, вып. 2, сс. 1743–1754, фев. 2000, doi: 10.1103/PhysRevE.61.1743.
26. R. D. Priestley, L. J. Broadbelt, J. M. Torkelson, K. Fukao, «Glass transition and alpha -relaxation dynamics of thin films of labeled polystyrene», *Phys. Rev. E Stat. Nonlin. Soft Matter Phys.*, vol. 75, is. 6 Pt 1, p. 061806, 2007, doi: 10.1103/PhysRevE.75.061806.
27. A. Sahnoune, L. Piché, «Glass Transition and Ultrasonic Relaxation in Polystyrene», *MRS Online Proc. Libr. OPL*, vol. 455, is. 183, 1996, doi: 10.1557/PROC-455-183.
28. J. Rieger, «The glass transition temperature of polystyrene: Results of a round robin test», *J. Therm. Anal.*, vol. 46, is. 3–4, p. 965–972, 1996, doi: 10.1007/BF01983614.
29. G.A. Slack, «Thermal Conductivity of II-VI Compounds and Phonon Scattering by Fe2+ Impurities», *Phys. Rev. B*6, is. 10, p. 3791–3800, 1972, doi: 10.1103/PhysRevB.6.3791.
30. S. Kasap, P. Capper, «Springer Handbook of Electronic and Photonic Materials.», Springer Handbooks, Springer International Publishing, 2017. doi: 10.1007/978-3-319-48933-9.
31. V.Litichevskyi, V.Tarasov, S.Galkin, O.Lalaiants, E.Voronkin, «Scintillation panels based on zinc selenide for detection alpha radiation», *Funct. Mater.*, vol. 19, is. 4, p. 546–550, 2012, http://www.functmaterials.org.ua/contents/19-4/fm194-22.pdf
32. Daniel C. Harris, Meghan Baronowski, Ladd Henneman, Leonard V. LaCroix, Clyde Wilson, Shelby C. Kurzius and others, «Thermal, Structural, and Optical Properties of Cleartran Multispectral Zinc Sulfide», *Optical Engineering 47(11)*, 2008, doi: 10.1117/1.3006123.
33. M.J. Reiney, M. Tryon, B.G. Achhammer, «Study of degradation of polystyrene, using ultraviolet spectrophotometry», *National Bureau of Standards*, Vol. 51, No. 3, p. 155, 1953, http://archive.org/details/jresv51n3p155
34. J.D. Peterson, S. Vyazovkin, C.A. Wight, «Kinetics of the Thermal and Thermo-Oxidative Degradation of Polystyrene, Polyethylene and Poly(propylene)», *Macromol. Chem. Phys.*, vol. 202, is. 6, p. 775–784, 2001, https://doi.org/10.1002/1521-3935(20010301)202:6%3C775::AID-MACP775%3E3.0.CO;2-G.
35. AMERICAN NATIONAL STANDARDS INSTITUTE, American National Standard for Dosimetry — Personnel Dosimetry Performance — Criteria for Testing, ANSI-N-13.11-1981, New York (1983)